Growth Kinetics of the Hydroxyapatite (0001) Face Revealed by Phase Shift Interferometry and Atomic Force Microscopy

Kazuo Onuma,*,†,‡ Noriko Kanzaki,§ Atsuo Ito,† and Tetsuya Tateishi†

National Institute for Advanced Interdisciplinary Research, 1-1-4 Higashi, Tsukuba, Ibaraki 305-8562, Japan, National Institute of Materials and Chemical Research, 1-1 Higashi, Tsukuba, Ibaraki 305, Japan and Institute of Earth Science, School of Education, Waseda University, Japan

Received: March 25, 1998; In Final Form: July 1, 1998

The relationship between the growth rate of the hydroxyapatite (0001) face and bulk supersaturation of a simulated body fluid was measured by real-time Moire phase shift interferometry. It was found that the (0001) face grew in the multiple two-dimensional nucleation mode, from surface observation by atomic force microscopy, and the growth rate data were fitted by the theoretical equation of multiple two-dimensional nucleation. The edge free energy of an island nucleated on the (0001) face, the most important parameter for two-dimensional nucleation, could be directly estimated as $\gamma = 3.3kT$, which was almost the same order as that on the (110) or (101) face of a lysozyme protein crystal.

Introduction

The growth mechanism of the hydroxyapatite ($Ca_{10}(PO_4)_6(OH)_2$; HAP) crystal, especially under physiological conditions, has been of great interest to many researchers.[1−5] Several papers have been published about the growth mechanism of HAP in terms of the relationship between the growth rate and supersaturation of the solution σ. For example, Koutsoukos et al.[6] found that the growth rate was proportional to $\sigma^{1.25}$ at low σ, by the constant composition method. Nancollas and Koutsoukos[7] investigated the growth rate at high σ and showed a linear relationship between the growth rate and σ. They concluded that the BCF spiral growth model[8] was applicable to HAP growth. Moreno et al.[9] and Moreno and Varughese[10] also arrived at the same conclusion on the basis of the results of a seeding growth experiment. Arends et al.,[11] on the other hand, found that the growth rate was proportional to $\sigma^{2.9-3.2}$ at neutral to slightly acidic pH. They emphasized the polynucleation mechanism.[12,13] Christoffersen and Christoffersen[14,15] investigated the previous data of HAP growth rate and fitted them to several theoretical rate equations. They concluded that the multiple two-dimensional nucleation mechanism was the most appropriate for HAP growth; however, the spiral growth mechanism was also applicable. Despite these efforts, no conclusive information about the growth mechanism of HAP is available. The main reason for this is undoubtedly the lack of direct surface observation and direct measurement of the growth rate of each face. Because the crystallographic face could not be clarified in the measurement of growth rate, information from all faces is averaged. This causes uncertainty in the estimation of important physical parameters, surface or edge free energies, from the growth rate measurements. Despite the anisotropic nature of these energies depending on the faces, we cannot obtain energetic information concerning the desired face. This situation arises owing to the difficulty of synthesizing large single crystals of HAP that can be utilized for surface observation, and the extremely slow growth rate as compared with those of soluble inorganic crystals. In the previous paper, we reported a new technique of measuring the growth rate of the HAP (0001), *c*-face, with high resolutions in space and time.[16] Using a hydrothermally synthesized large single HAP crystal as a seed,[17] the normal growth rate of the *c*-face was directly measured for the first time by the Moire phase shift interferometric technique. Combined with surface observation by atomic force microscopy (AFM), the *c*-face was found to grow in the multiple two-dimensional nucleation mode in a simulated body fluid. In this study, we investigate the growth rate dependence on the supersaturation of the solution in order to understand the growth mechanism more clearly, and the edge free energy, the most important parameter for two-dimensional nucleation, is calculated to clarify the features of HAP growth. Surface observation by AFM is also employed to determine the point of critical supersaturation above which nucleation begins to occur.

Experimental Section

1. Moire Phase Shift Interferometry. The schematic drawing of the Moire phase shift interferometry and signal-processing route to calculate the two-dimensional phase distribution profile of the surface, which is proportional to the three-dimensional height profile, is shown in Figure 1. Since the details of the interferometry were already described in the previous paper,[16] only a brief explanation is given. It is the common-path-type interferometry using a Nomarsky prism. The interferogram of the crystal surface is input to the signal processor and converted to the two-dimensional phase distribution map after Moire processing combining with three digitally composed reference interferograms whose phases are shifted 90° to each other. After Moire processing, three interferograms, I_j ($j = 1, 2, 3$), with phase shift of 90° to each other are obtained. From these interferograms, the two-dimensional phase distribution, $\phi(x, y)$, of the crystal surface is calculated using

$$\phi(x, y) = \tan^{-1}\{(I_3 - I_2)/(I_1 - I_2)\} + \pi/4^{18} \qquad (1)$$

The three-dimensional height profile, $h(x, y)$, can be related to $\phi(x, y)$ as

* To whom correspondence should be addressed. Tel.: +81-298-54-2557. Fax: +81-298-54-2565. E-mail: onuma@nair.go.jp.
† National Institute for Advanced Interdisciplinary Research.
‡ National Institute of Materials and Chemical Research.
§ Waseda University.

S1089-5647(98)01617-4 CCC: $15.00
Published on Web 09/10/1998

$$h(x, y) = \lambda/4\pi n \times \phi(x, y) \quad (2)$$

where λ and n are the wavelength of the laser and the refractive index of the solution, respectively.[19]

2. Atomic Force Microscopy. Surface observation of the *c*-face growth process was carried out using a NanoScope III-a AFM (Digital Instruments) in the tapping mode using the J-type piezo scanner with a 100 μm scanning range. Silicon single-crystal cantilevers with spring constants of 20−50 N/m were applied in all observations.

3. Solution Composition and Seed Crystal. The pseudo-physiological solutions used in this study contain NaCl as the background electrode, $CaCl_2$ and $K_2HPO_4 \cdot 2H_2O$ as the source for the growth of HAP, and trisaminomethane (Tris) and HCl as the buffer to maintain the pH of the solutions at 7.4. The basic solution contains 140 mM NaCl, 2.5 mM $CaCl_2$, 1 mM $K_2HPO_4 \cdot 2H_2O$, and 50 mM Tris, so-called "Kokubo solution[20]". Supersaturation of the solutions is achieved by changing the amount of each reagent in the same proportion as the basic solution.

The large single HAP crystal used as a seed was synthesized by hydrothermal techniques. Details of the synthesis can be found in ref 17. The representative composition of the single crystal used in this work is CaO, 55.3 wt %; P_2O_5, 41.9 wt %; CO_2, 0.09 wt %, and the Ca/P ratio is 1.67.

The whole system of the interferometry and the growth cell are put in the thermostated room, and the temperature of the solution is kept constant at 25 °C in each growth rate measurement.

4. Definition of Supersaturation. Supersaturation of the solution is calculated using

$$\sigma = ((C - C_e)/C_e) = (I_p/K_{sp})^{1/18} - 1 \quad (3)$$

where σ is the bulk supersaturation of the solution, C and C_e, are actual and equilibrium concentrations, respectively, and I_p and K_{sp} are ionic activity of the solution and solubility product of HAP, respectively. We used the value of 10^{-119} as K_{sp}, and I_p was calculated using the program in ref 21. The supersaturation range in the present study is 0.85−22.0. Although the σ is high, the solution is stable more than one week without any spontaneous three-dimensional nucleation, which is confirmed by several measurement of the growth rate at different periods under the same σ. The Tris-buffer may have some role in stabilizing the solution at high supersaturation. Since σ is much higher than unity, it is related to the chemical potential difference between the crystal and the solution, $\Delta\mu$, as $\ln(1 + \sigma) = \Delta\mu/kT$.

Results

1. Surface Observation by AFM. Figure 2 shows the surface morphology of the *c*-face after growth in the solution with $\sigma = 22.0$. Figure 2a shows the image of the seed surface, Figure 2b the surface image after 5 min of growth, and Figure 2c the image after 2 h of growth. It can be seen, in Figure 2b, that many small islands, about 5−10 nm in diameter, are nucleated on the surface. Although the height of islands is difficult to define owing to the undulation of the seed surface, it can be said that the minimum height of the islands seen in Figure 2b is of the order of 1 nm as shown in the high magnification image with the section profile of one island in Figure 2c. These islands grow in both lateral and vertical directions and form uniform islands of 30−40 nm in diameter and about 5−6 nm in height after 2 h of growth. Smaller islands, as seen in Figure 2b, should be formed in Figure 2c, although they are difficult to distinguish. This feature of growth does not change with supersaturation under the present conditions. As revealed by the X-ray photoelectron spectroscopic study in the previous work,[16] the Ca/P ratio of grown phase was 1.19−1.25 depending on the growing time. The Ca/P ratio of the seed crystal was simultaneously measured and found as 1.32. Because the real Ca/P ratio of the seed crystal was 1.66−1.67,[17] the real Ca/P ratio of the grown phase was 1.50−1.60 using the Ca/P ratio of the seed as the reference. The grown material on the seed is calcium-deficient HAP with low crystallinity.

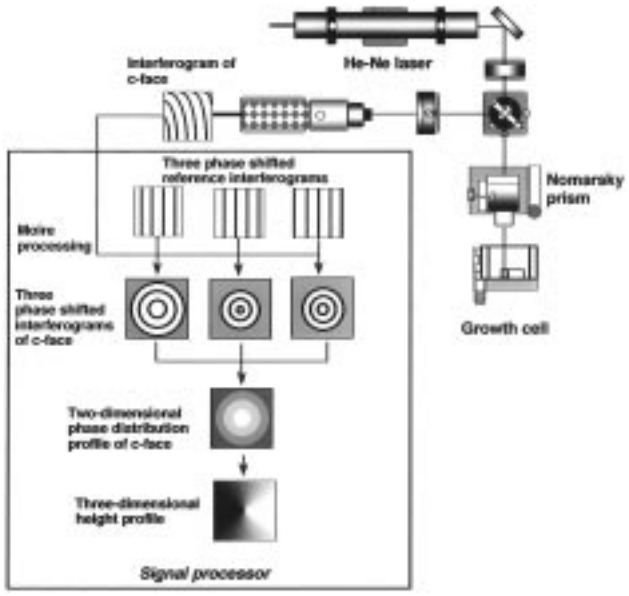

Figure 1. Schematic drawing of shearing-type Moire phase shift interferometry and signal-processing route for calculation of a two-dimensional phase distribution profile of the growing crystal surface.

2. Observation by Moire Phase Shift Interferometry. Figure 3 shows an example of the crystal surface observed by the present Moire phase shift interferometry. Figure 3a shows the original interferogram of the surface with vertical concentrated fringes to be converted to a real surface profile after Moire processing. Figure 3b is the two-dimensional phase distribution profile obtained after Moire processing using the original interferogram and the reference interferogram, which is created in the signal processor. In Figure 3b, a two-dimensional phase distribution profile is expressed as a gray level image. Quantitative phase data at each pixel of the CCD camera are, of course, stored in the memory simultaneously. Figure 3c shows the three-dimensional height plot using the data in Figure 3b. The growth rate in each position of the surface is calculated by monitoring the change of the phase, which is proportional to the relative height, as mentioned in a previous section, depending on time. All processes for calculating phase values are finished with a TV rate, 1/30 s.

3. Growth Rate versus Time. The growth rate of the *c*-face was found to be strongly dependent on time. We measure the growth rate as a function of time over the entire supersaturation range to confirm whether the relationship between the growth rate and time seen in the previous work[16] holds or not. Figure 4a shows the result for three representative supersaturations, $\sigma = 9.8$, 14.0, and 22.0. For all σ, the relative change in height decreases with time and becomes constant as late as after about 24 h of growth. The growth rate at each time, therefore, gradually decreases with time, and, finally, growth almost stops. This feature is not attributed to the decrease of the solution

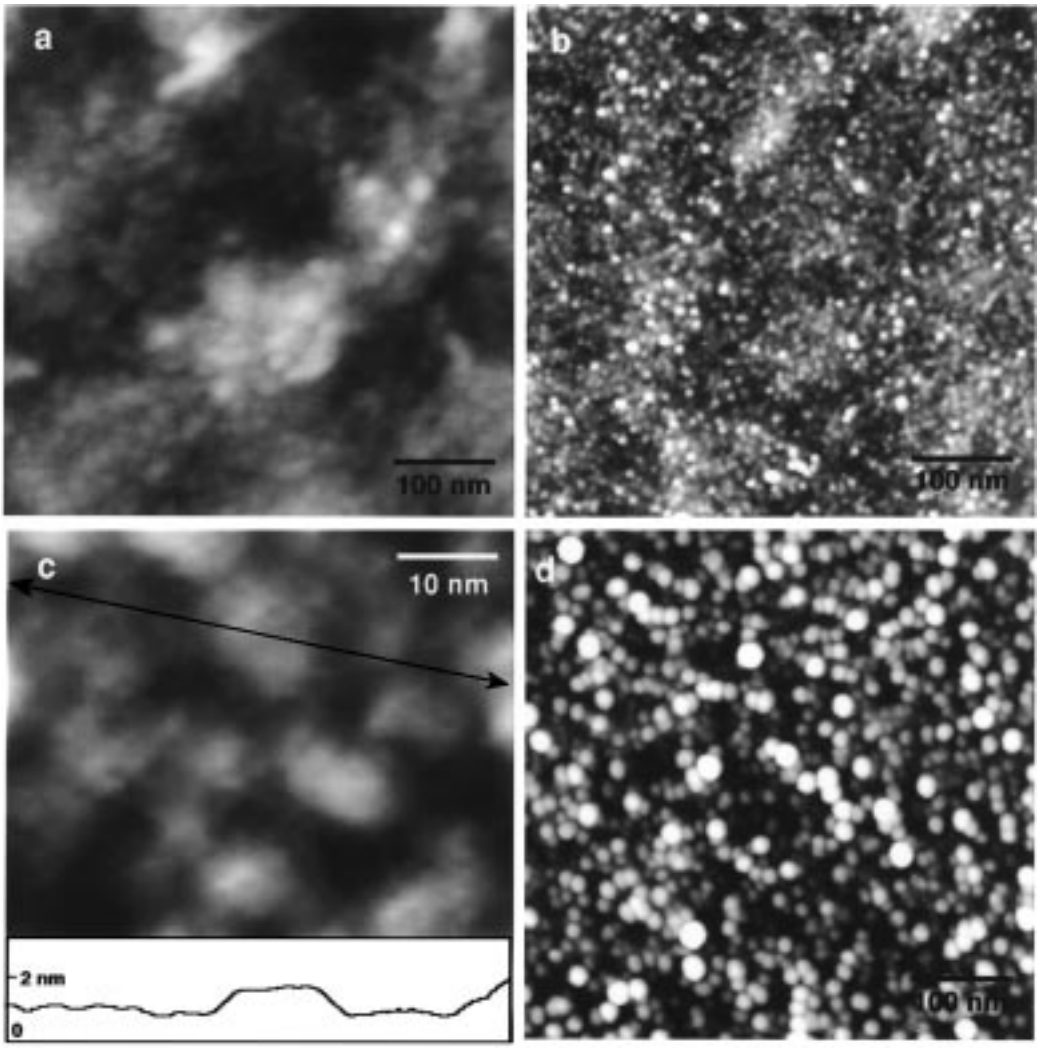

Figure 2. Surface morphologies of the *c*-face growing on the solution, $\sigma = 22.0$. (a) Seed surface. (b) The surface after 5 min of growth. Small islands, 5−10 nm in diameter nucleated on the surface. (c) High-magnification image of Figure 2b with the section profile of the island. (d) Surface after 2 h of growth. The islands increase to 30−40 nm in diamter.

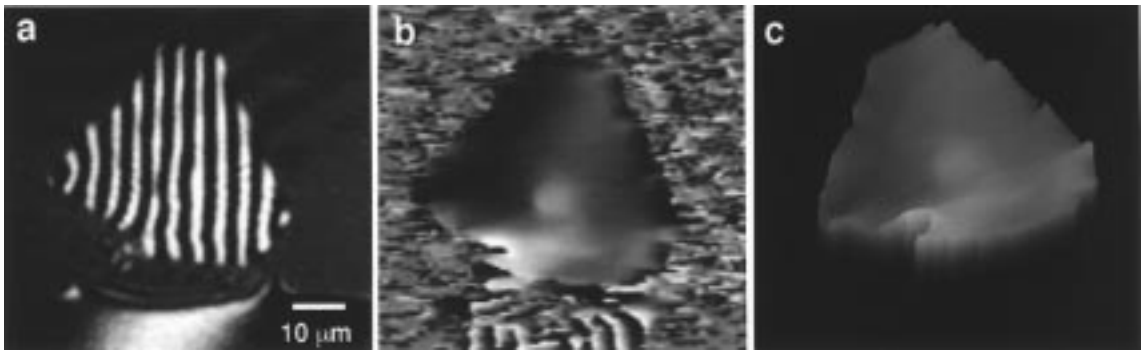

Figure 3. Example of surface topography processed by Moire phase shift interferometry: (a) original interferogram of the *c*-face; (b) two-dimensional phase distribution image after Moire phase shift processing in the signal processor; (c) three-dimensional height plot using the data in (b).

concentration, which was already confirmed using the ICP method as mentioned in our previous paper.[16] Although the total thickness of the grown layer on the seed seems to depend on the supersaturation, based on Figure 4a, several measurements for different crystals indicate that the total thickness of the grown layer does not show a definitive dependence on supersaturation, and is almost constant at around 400−700 nm, as shown in Figure 4b. As mentioned in the previous paper, we fit the data using a simple polynomial function, and the growth rate is defined as the slope of the tangent line at $t = 0$.

4. Growth Rate versus Supersaturation. Figure 5 shows the relationship between the growth rates of the *c*-face and supersaturation of the solution. The growth rate increases above $\sigma = 9.8$. For each σ, the growth rates are measured several times for different seed crystals and the data are obtained from several positions on the surface. The dispersion of the growth rates is different depending on σ; however, these are fitted within the maximum error of 20%. For $\sigma < 9.8$, we have not yet suceeded in obtaining relaible data of the growth rate because the fluctuation in room temperature severely affects the fringe

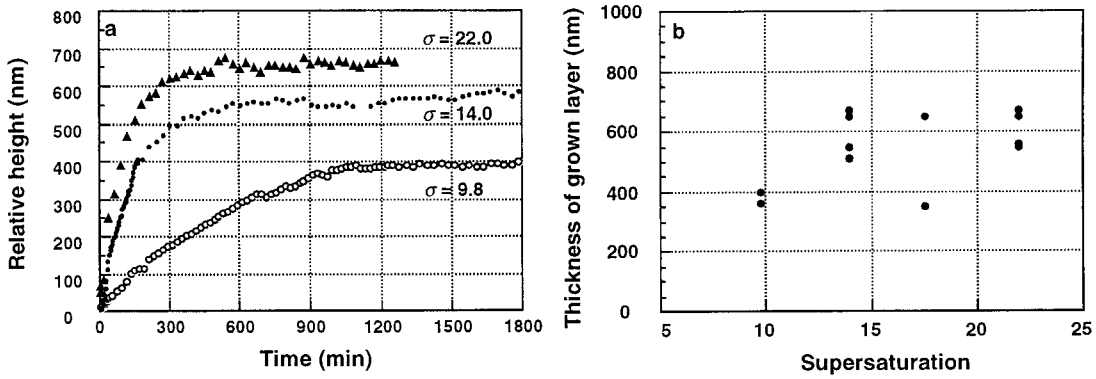

Figure 4. (a) Relationship between the increase of relative height of the *c*-face and time at various supersaturations. Note that the growth rates strongly depend on time and finally are almost negligible. (b) Total thickness of the grown layer in relation to the supersaturation of the solution.

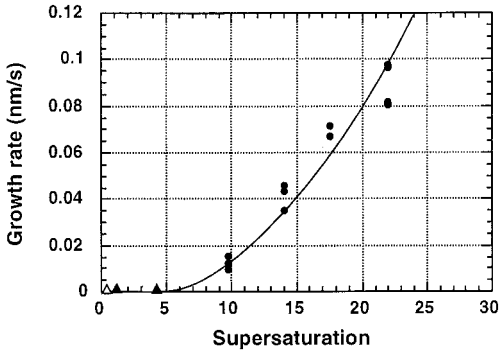

Figure 5. Relationship between the growth rate of the *c*-face and the supersaturation of the solution. Closed circles indicate the measured value, closed triangles indicate that the growth is confirmed by AFM observation, but the measurement of growth rate is not yet successful, and open triangles indicate no sign of growth.

movement because of the thermal drift of the aluminum stages that hold the growth cell and the Nomarsky prism. However, determining the critical σ, σ_c, above which nucleation begins to occur, is important. Since interferometric measurement cannot be applied around σ_c, we observed the surface profile using AFM to estimate σ_c. In Figure 5, closed triangles indicate that two-dimensional nucleation growth was confirmed by surface observation with AFM although the growth rates were not measured. In contrast, open triangles indicate that there is no sign of growth. For example, Figure 6 shows the surface features after 5 h of growth at $\sigma = 0.85$ combined with the surface morphology of the seed crystal (Figure 6a). It can be seen that the islands begin to nucleate at $\sigma = 0.85$ as shown by arrows (Figure 6b), whereas the growth was not observed at $\sigma = 0.4$. On the basis of this result, we judge σ_c as the intermediate between 0.4 and 0.85, $\sigma_c = 0.6$.

Discussion

From the surface observation by AFM, it was found that the *c*-face grew in the multiple two-dimensional nucleation mode under the present conditions. The growth rate, *R*, in multiple two-dimensional nucleation[12,13] is as follows when we take the anisotoropic morphology of the growth unit into consideration. In the following equations, we assume the growth unit to be polygonal with the side length *a* and the height *h*, which are constant during the growth.

$$R = h(\pi V^2 J/3)^{1/3} \tag{4}$$

where $V = \omega C_e \beta \sigma$ is the step velocity of the nucleated island with the height *h*. ω is the specific molecular volume of HAP, and C_e and β are the equilibrium concentration of HAP, which can be expressed by K_{sp}, and the step kinetic coefficient, respectively.

The formation rate of two-dimensional nuclei, *J*, is

$$J = B \exp(-\pi\alpha^2\omega h/kT\Delta\mu) = B \exp\{-\pi\alpha^2\omega h/(kT)^2 \ln(1+\sigma)\} \tag{5}$$

where α is the surface free energy at a step that can be related to edge free energy, γ, using *h* and ω, as $\gamma = \alpha(h\omega)^{1/2}$.

The factor *B* is

$$B = Z(2\pi NC\omega\gamma/\Delta\mu)\nu \exp(-E/kT) \tag{6}$$

where *Z* is the Zeldovich factor, *N* is a constant, *C* is the concentration of the solution, and *E* is the activation energy required for the incorporation of a new growth unit into the nucleus, given in terms of the β as $\beta = a\nu \exp(-E/kT)$. Because $Z = (\Delta\mu)^{3/2}/4\pi\gamma\,(kT)^{1/2}$, *B* can be expressed as

$$B = {}^1/_2 N\omega C_e \nu \exp(-E/kT)(1+\sigma)\{\ln(1+\sigma)\}^{1/2} \times \exp\{-\pi\gamma^2/(kT)^2 \ln(1+\sigma)\} \tag{7}$$

The growth rate, *R*, is thus

$$R = K\sigma^{2/3}(1+\sigma)^{1/3}\{\ln(1+\sigma)\}^{1/6} \times \exp[-\pi\gamma^2/\{3(kT)^2 \ln(1+\sigma)\}] \tag{8}$$

where *K* is a constant incorporating *E*.

The equation above can be transformed into a linear equation by considering the relationship between $\ln[R/[\sigma^{2/3}(1+\sigma)^{1/3}\{\ln(1+\sigma)\}^{1/6}]]$ versus $1/\ln(1+\sigma)$ as follows.

$$\ln[R/[\sigma^{2/3}(1+\sigma)^{1/3}\{\ln(1+\sigma)\}^{1/6}]] = \ln K - \{\pi\gamma^2/3(kT)^2\} \times 1/\ln(1+\sigma) \tag{9}$$

From the slope of the plot of $\ln[R/[\sigma^{2/3}(1+\sigma)^{1/3}\{\ln(1+\sigma)\}^{1/6}]]$ against $1/\ln(1+\sigma)$, the edge free energy, γ, can be obtained. Figure 7 indicates the relationship between $\ln[R/[\sigma^{2/3}(1+\sigma)^{1/3}\{\ln(1+\sigma)\}^{1/6}]]$ and $1/\ln(1+\sigma)$ recalculated from the data used in Figure 5. It is clear that all data lie on the straight line with the correlation coefficient, $r^2 = 0.9$. The slope of the line is found to be 11.5; thus, γ is 1.36×10^{-13} erg. Because γ changes with temperature, it is useful to express γ using the Boltzmann constant and absolute temperature as $\gamma = 3.3kT$. This value is much larger than those reported in previous papers based on indirect growth rate measurements. Although the crystal face was not specified in the previous studies, γ values were in the range of $1.12kT-1.95kT$, which are about

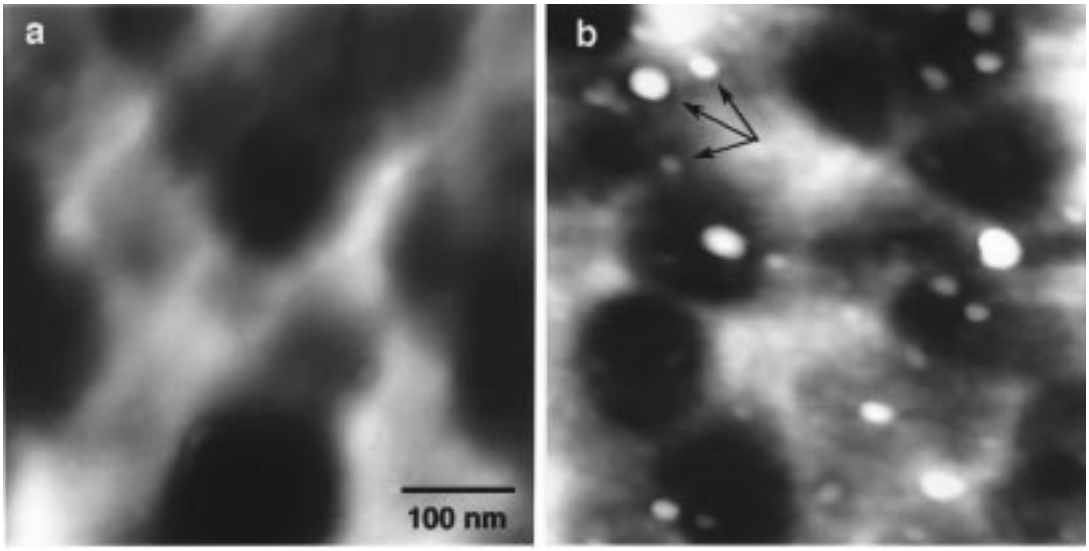

Figure 6. Surface morphologies of *c*-face around critical supersaturation above which the two-dimensional nucleation begins to occur. (a) Seed surface. (b) The surface after 5 h of growth at $\sigma = 0.85$. The islands start to grow as shown by arrows.

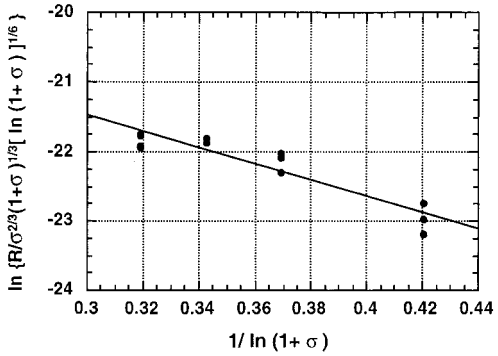

Figure 7. Logarithmic plot of the growth rate for the calculation of the edge free energy.

half of our value if we assume that the observed faces were the same. The reason for this may be related to the supersaturation in HAP growth. The supersaturation used in the growth rate measurement is 9.8−22, whereas, in previous studies, the supersaturation was lower, 0.4−7. With low supersaturation, the heterogeneous nucleation effect increases, as Malkin et al. pointed out, in ADP growth.[22] They investigated nucleation growth of the ADP (101) face and estimated the surface energy. The result showed that the surface energy changed irregularly at critical supersaturation. The surface energy calculated from the growth rates at high supersaturation was about three times larger than that calculated from the growth rates at low supersaturation. They concluded that impurity particles adsorbed on the surface acted as heterogeneous nucleation centers in low supersaturation and decreased the surface energy, and hence the edge free energy. The same phenomenon was observed for the (100) face of the $Ba(NO_3)_2$ crystal.[23] In the case of the HAP crystal, therefore, it is also possible that heterogeneous nucleation occurred at low supersaturation and decreased the calculated edge free energy. Indeed, the estimated σ_c in Figure 6 does not correspond to the value extrapolated from the relationship between growth rate and supersaturation in Figure 5, indicating that the growth rate dependence on the supersaturation for $\sigma < 9.8$ is much gentler and, hence, the edge free energy calculated using the growth rate data in this region should be smaller than the present value, $\gamma = 3.3kT$.

The γ value obtained in the present study is very interesting compared with those of other aqueous solution grown crystals. As described earlier, Malkin et al.[22] investigated the growth feature of the (101) face of the ADP crystal, which is the representative soluble inorganic crystal, by the interferometric technique and found the surface free energy at the step, α, to be 11.8 erg/cm^2, under homogeneous two-dimensional nucleation growth. Thus, γ on the ADP (101) face can be expressed as $\gamma = 0.7kT$. On the other hand, γ of the macromolecular protein crystal was investigated by Durbin and Feher,[24] and Sazaki et al.[25] on lysozime (110) and (101) faces and found to be $\gamma = 3.8kT$ and $2.8kT$, respectively. Although the HAP is an ordinary inorganic crystal, the edge free energy is about 4−5 times larger than that of soluble inorganic crystals and is very close to that of a protein crystal when we compare the edge free energies of these crystals on the faces in which the growth proceeds in the homogeneous two-dimensional nucleation mode. The energetic barrier for two-dimensional nucleation is roughly proportional to γ^2; thus, a higher supersaturation is necessary for the HAP crystal to start nucleation than in the case of small molecular inorganic crystals, which is similar to the case of a protein crystal. The reason for the high γ value on the HAP (0001) face is usually attributed to the high surface energy. Because γ can be related to the surface energy α as $\gamma = \alpha(h\omega)^{1/2}$, the high surface energy at the step due to the structure of the step front results in a high γ value although the exact structure of the step front cannot be clearly understood. In this case, the observed thick step in Figure 2c may result from the step bunching by impurities, and the AFM could not resolve each thinner step. However, we would like to point out the second possibility that the high h and ω can also result in a high γ value. This situation occurs if the growth unit of HAP is not small ionic species but large clusters, when we assume that the step height of two-dimensional nuclei is the height of one growth unit. In previous works,[26,27] we measured the step kinetics of the HAP *a*-face by in situ AFM and found that the step kinetic coefficient, corresponding to the resistance for incorporation of the growth unit at a step front, is of the same order as those of protein and virus crystals. On the basis of these results, we assumed that the HAP does not grow with ionic growth units but with cluster of growth unit. This hypothesis was confirmed by a dynamic light scattering study for simulated body fluids in which the HAP grew,[28] and one of the authors presented the growth model of HAP based on the Posner cluster,[29] $Ca_9(PO_4)_6$, 0.8 nm in diameter, as the growth

unit. These results strongly support the second reason for the high experimentally calculated γ value in the present study.

Acknowledgment. This study was supported by AIST (Agency of Industrial Science and Technology). The authors thank K. Teraoka for preparing the HAP single crystals.

References and Notes

(1) Murphy, B. T.; Pyrah, L. N. *Br. J. Urol.* **1962**, *34*, 129.
(2) Schoen, F. J.; Harasaki, H.; Kim, K. M.; Anderson, C.; Levy, R. J. *J. Biomed. Mater. Res., Appl. Biomater*. **1988**, *22 A1*, 11.
(3) Mann, S.; Webb, G.; Williams, R. J. P. *Biomineralization*; VCH Verlagsgesellschaft: Weinheim, 1989.
(4) Hench, L. L.; Wilson, J. *An introduction to bioceramics*; World Scientific: Singapore, 1993.
(5) Doherty, T. M.; Detrano, R. C. *Calcif. Tissue Int.* **1994**, *54*, 224−230.
(6) Koutsoukos, P. G.; Amjad, Z.; Tomson, M. B.; Nancollas, G. H. *J. Am. Chem. Soc*. **1980**, *102*, 1553.
(7) Nancollas, G. H.; Koutsoukos, P. G. *Prog. Cryst. Growth Charact.* **1980**, *3*, 77.
(8) Burton, W. K.; Cabrera, N.; Frank, F. C. *Philos. Trans. R. Soc. London A* **1951**, *243*, 299.
(9) Moreno, E. C.; Zahradnik, R. T.; Glazman, A.; Hwu, R. *Calcif. Tissue Res.* **1977**, *24*, 47.
(10) Moreno, E. C.; Varughese, K. *J. Cryst. Growth* **1981**, *53*, 20.
(11) Arends, J.; Christoffersen, J.; Christoffersen, M. R.; Eckert, H.; Fowler, B. O.; Heughebaert, J. C.; Nancollas, G. H.; Yesinowskl, J. P.; Zawacki, S. J. *J. Cryst. Growth* **1987**, *84*, 515.
(12) Chernov, A. A. In *Modern Crystallography III*: *Crystal Growth*; Vainshtein, B. K., Chernov, A. A., Shuvalov, C. A., Eds.; Springer: Berlin, 1984.
(13) Markov, I. V. In *Crystal Growth for beginners*: *Fundamental of Nucleation, Crystal Growth and Epitaxy*; World Scientific Publishing Co. Pte. Ltd.: Singapore, 1995.
(14) Christoffersen, M. R.; Christoffersen, J. *J. Cryst. Growth* **1992**, *121*, 608.
(15) Christoffersen, M. R.; Christoffersen, J. *J. Cryst. Growth* **1992**, *121*, 617.
(16) Kanzaki, N.; Onuma, K.; Ito, A.; Teraoka, K.; Tateishi, T.; Tsutsumi, S. Submitted to *J. Phys. Chem. B.*
(17) Ito, A.; Nakamura, S.; Aoki, H.; Akao, M.; Teraoka, K.; Tsutsumi, S.; Onuma, K.; Tateishi, T. *J. Cryst. Growth* **1996**, *163*, 311.
(18) Nakadate, S.; Yamaguchi, I. Japanese Patent laid-open H02-287107, 1990.
(19) Onuma, K.; Kameyama, T.; Tsukamoto, K. *J. Cryst. Growth* **1994**, *137*, 610.
(20) Kokubo, T.; Kushitani, H.; Sakka, S.; Kitsugi, T.; Yamamoto, T. *J. Biomed. Mater. Res.* **1990**, *24*, 721.
(21) Maekawa, K. M.S. Thesis, Waseda University, Tokyo, Japan, 1995.
(22) Malkin, A. I.; Chernov, A. A.; Alexeev, I. V. *J. Cryst. Growth* **1989**, *97*, 765.
(23) Maiwa, K. *Proceedings of the Fourth Topical Meeting on Crystal Growth Mechanism*, Tokyo, 1991.
(24) Durbin, S. D.; Feher, G. *J. Cryst. Growth* **1986**, *76*, 583.
(25) Sazaki, G.; Kurihara, K.; Miyashita, S.; Komatsu, H.; Nakada, T. *J. Jpn. Assoc. Cryst. Growth* **1996**, *23* (5), 41.
(26) Onuma, K.; Ito, A.; Tateishi, T.; Kameyama, T. *J. Cryst. Growth* **1995**, *154*, 118.
(27) Onuma, K.; Ito, A.; Tateishi, T. *J. Cryst. Growth* **1996**, *167*, 773.
(28) Onuma, K.; Ito, A. Submitted to *Chem. Mater.*
(29) Posner, A. S.; Betts, F. *Ac. Chem. Res.* **1975**, *8*, 273.